

Engineering of Mature Human Induced Pluripotent Stem Cell-Derived Cardiomyocytes Using Substrates with Multiscale Topography

Parisa P. S. S. Abadi, Jessica C. Garbern, Shahed Behzadi, Michael J. Hill, Jason S. Tresback, Tiam Heydari, Mohammad Reza Ejtehadi, Nafis Ahmed, Elizabeth Copley, Haniyeh Aghaverdi, Richard T. Lee, Omid C. Farokhzad, and Morteza Mahmoudi*

Producing mature and functional cardiomyocytes (CMs) by in vitro differentiation of induced pluripotent stem cells (iPSCs) using only biochemical cues is challenging. To mimic the biophysical and biomechanical complexity of the native in vivo environment during the differentiation and maturation process, polydimethylsiloxane substrates with 3D topography at the micrometer and sub-micrometer levels are developed and used as cell-culture substrates. The results show that while cylindrical patterns on the substrates resembling mature CMs enhance the maturation of iPSC-derived CMs, sub-micrometer-level topographical features derived by imprinting primary human CMs further accelerate both the differentiation and maturation processes. The resulting CMs exhibit a more-mature phenotype than control groups—as confirmed by quantitative polymerase chain reaction, flow cytometry, and the magnitude of beating signals—and possess the shape and orientation of mature CMs in human myocardium—as revealed by fluorescence microscopy, Ca²⁺ flow direction, and mitochondrial distribution. The experiments, combined with a virtual cell model, show that the physico-mechanical cues generated by these 3D-patterned substrates improve the phenotype of the CMs via the reorganization of the cytoskeletal network and the regulation of chromatin conformation.

1. Introduction

Myocardial infarction (MI) is one of the main causes of heart failure worldwide.^[1] MI induces extensive damage to cardiomyocytes (CMs) in the affected myocardium. The pre-infarcted area of myocardium contains a large portion of stunned CMs, which may be capable of recovery if exposed to reoxygenation, therapeutic drugs, and/or paracrine factors.^[2] Though CM renewal occurs in a post-natal heart, the capacity for regeneration is limited and decreases significantly with age.^[3] Cell-therapy and tissue-engineering approaches have been used to develop solutions to this problem.^[2a,4] However, acquiring a viable source of patient-specific CMs remains a major limitation due to the limited in vitro expansion potential of CMs.^[3] Furthermore, patient-specific CMs are needed to minimize immune rejection of the therapeutic cells.^[2a] In light of these

Prof. P. P. S. S. Abadi, Dr. S. Behzadi, E. Copley, Dr. H. Aghaverdi, Prof. O. C. Farokhzad, Dr. M. Mahmoudi
Center for Nanomedicine and Department of Anesthesiology
Brigham and Women's Hospital
Harvard Medical School
Boston, MA 02115, USA
E-mail: mmahmoudi@bwh.harvard.edu

Prof. P. P. S. S. Abadi, Dr. M. J. Hill
Department of Mechanical Engineering-Engineering Mechanics
Michigan Technological University
Houghton, MI 49931, USA

Dr. J. C. Garbern
Department of Cardiology
Boston Children's Hospital
Boston, MA 02115, USA

 The ORCID identification number(s) for the author(s) of this article can be found under <https://doi.org/10.1002/adfm.201707378>.

^[†]Present address: Department of Physics and Astronomy
University of British Columbia Vancouver, BC, Canada V6T 1Z1

Dr. J. C. Garbern, N. Ahmed, Prof. R. T. Lee
Department of Stem Cell and Regenerative Biology
Harvard University
Harvard Stem Cell Institute
Cambridge, MA 02138, USA

J. S. Tresback
Center for Nanoscale Systems
Harvard University
Cambridge, MA 02138, USA

T. Heydari,^[†] Prof. M. R. Ejtehadi
Department of Physics
Sharif University of Technology
Tehran 11155-8639, Iran

Prof. R. T. Lee
Department of Medicine
Division of Cardiology
Brigham and Women's Hospital and Harvard Medical School
Cambridge, MA 02138, USA

DOI: 10.1002/adfm.201707378

facts, it has been recognized that induced pluripotent stem cells (iPSCs) are a promising source of CMs that avoids the ethical issues surrounding embryonic stem cells (ESCs).^[5] Transplantation of CMs that are differentiated from iPSCs (iCMs) is preferable to direct use of iPSCs due to the enhanced functionality and reduced risk of tumor formation.^[6] In addition to their therapeutic benefits in myocardial salvage and regeneration, iCMs have also demonstrated great potential to simulate myocardium for the purposes of drug screening (e.g., chemotherapeutic drugs in cancer patients), and have proven superior to other approaches including neonatal nonhuman cells due to the inherent physiological differences between species.^[7] Finally, CMs are excellent bioactuators, capable of transforming electrical signals into mechanical work in biorobotics applications.^[8]

Transplantation of CM or stem cell suspensions is an emerging treatment for damaged myocardium via injection of cells into the preinfarcted area. However, in addition to low retention of injected cells in the myocardium, a challenge is the immature nature of the CMs that do survive, compared to their native counterparts.^[9] Native CMs have a cylindrical shape, a length-to-width ratio of ≈ 7 , a sarcomeric length of 2 μm , cell volume occupied by mitochondria arranged in a lattice pattern (more than 20% of the volume), and individual cell contractility on the μN scale.^[10] Changes in these fundamental parameters signify a pathological state, with reduced potential for cell shortening and contractility. iCMs typically display signs of immaturity such as reduced aspect ratio, shorter sarcomere length, and fewer mitochondria.^[10b,11] This immature morphology is evident even after *in vitro* differentiation of the iPSCs according to standard protocols, indicating that the biochemical signals used to induce differentiation do not suffice for maturation.^[11c] On top of this, while iCMs derived from both ESCs and iPSCs suffer from immaturity, there is some evidence that those derived from iPSCs are even less mature than those derived from ESCs.^[12] Therefore, methods that enhance the maturation of iCMs from iPSCs prior to injection or drug screening tests are crucially needed. It has also been the consensus that the differentiation process suffers from batch-to-batch variation and lack of repeatability.^[13] Accordingly, it is logical to conclude that the physical cues provided to iPSCs during standard culture conditions do not sufficiently mimic the natural process of differentiation to fully mature CMs.

One promising method intended to remedy this situation is the patterning of culture substrates. It has been known since the early 20th century that cells cultured *in vitro* respond to topological features of the culturing substrate when they are of the appropriate scale to be relevant to the cell.^[14] This process of patterning—haptotaxis in the case of surface energy gradients or contact guidance, in the case of topological patterns only—has been utilized to promote the maturity of iCMs.^[15] Continuous surface grooves have been proven effective to align CMs and increase anisotropic contractility, which better mimics native myocardium.^[16] However, this method has fallen short in engineering individual CMs with the proper aspect ratio. Surfaces with 2D rectangular patterns with an aspect ratio of 7 enhance the maturity of CMs, as demonstrated by both increased contractility and aligned sarcomeric structures.^[10a]

In vivo, however, cells do not exist in 2D; they are embedded within a complex 3D matrix that provides a unique context and conditions for both cell shape and behavior.^[17] Therefore, creating a 3D pattern that mimics natural cell-surface features at both the micro- and nanoscale might provide epigenetic cues that more closely mimic the native multiscale environment of the iCM and promote a more physiologically mature phenotype.

Cell imprinting has emerged from attempts at molecular imprinting of gels and polymers to create selectively adsorbent materials.^[18] The field of cell imprinting seeks to create substrates that selectively capture or separate bacteria and other cells.^[19] However, recent applications have moved toward imprinting as a means of guiding the behavior of cultured cells by controlling their adhesive interactions with surfaces. While one previous study demonstrated that bacterial cell imprinting was dependent on the chemistry of the imprinted material, another study showed that, at least for mammalian stem cells, the effects of imprinting remained when the surface chemistry of the originally imprinted surface was screened.^[18b,20] The mechanisms behind the effects of cell imprinting for mammalian cells may be related to the requirement for cytoskeletal rearrangement and local fitting of the cell membrane to surfaces on the nanoscale, which *in vivo* is facilitated by the imprints of other cells and consequent changes in nucleus shape (via linkage of nucleoskeleton and cytoskeleton proteins) and chromatin conformation.^[21] Though *in vitro* cell imprinting previously utilized the imprints of cells cultured on 2D surfaces to control the fate of mesenchymal stem cells, we sought to imprint more physiological features by imprinting cells cultured on a 3D patterned surface to either induce maturation of the iCMs or better direct the fate of iPSCs to iCMs.^[20a]

Here, we employed photolithography and cell imprinting to produce scaffolds with 3D features that mimic the physiological shape and surface features of mature CMs. Our scaffolds replicate the micro- and nanoscale features of mature human CMs. With this method, we sought to achieve the three following objectives: (i) to enhance cell reprogramming from iPSCs to iCMs, (ii) to induce the physiological 3D shape and orientation of iCMs, and (iii) to produce mature and highly functional CMs.

2. Results

We fabricated polydimethylsiloxane (PDMS) substrates to function as scaffolds capable of physical guidance of orientation and maturation of iCMs differentiated from iPSCs, as well as to facilitate differentiation of CMs from iPSCs (schematically shown in **Figure 1a**). First, via photolithography, we created aligned microgrooves resembling the physiological dimensions of individual mature CMs: 100 μm in length and an aspect ratio of ≈ 7 (**Figure 1b**). To create the patterns in the PDMS, a continuous layer of a positive photoresist (AZ4620) was initially deposited on a Si wafer and patterned by UV using a photo-mask. A thermal reflow process was used to transform the micromolds to semicylinders before use in formation of microgrooves in PDMS (**Figure 1c**). In the next step, we extended the fabricated topography from the micrometer to sub-micrometer level. Mature primary human CMs seeded on polystyrene

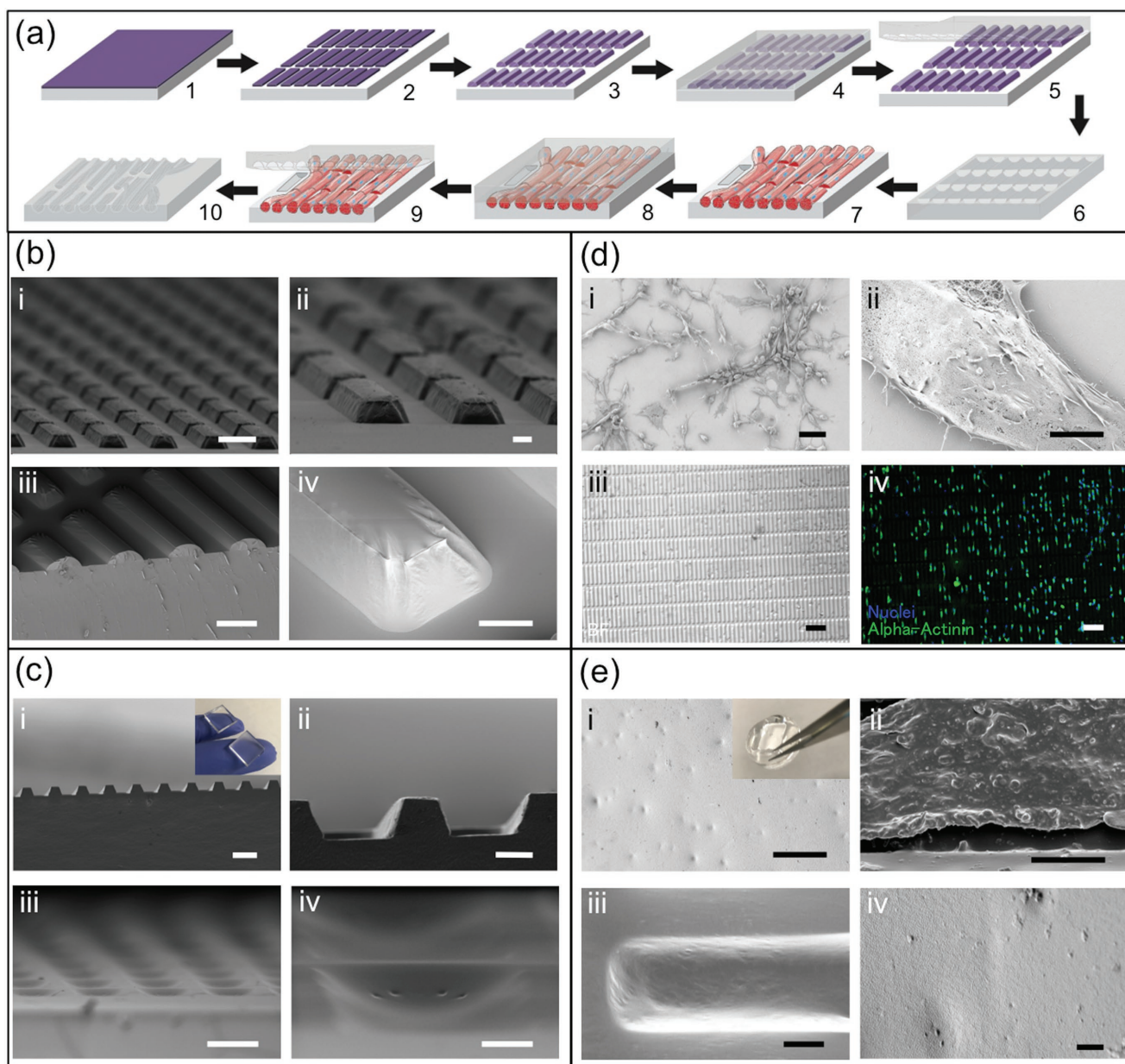


Figure 1. Microfabrication and cell imprinting for fabrication of substrates. a) Schematic representation of the microfabrication and cell-imprinting process: (1) Deposition of photoresist, (2) photolithography patterning of the photoresist, (3) formation of semicylinders by reflow process, (4) PDMS coating of the hard mold by drop-casting, (5) removal of PDMS, (6) micropatterned PDMS substrate is ready for cell seeding, (7) human primary cardiomyocytes are seeded on micropatterned PDMS substrate, (8) PDMS coating of primary cardiomyocytes, (9) removal of the PDMS coating, and (10) cell-imprinted PDMS substrate is ready for use as scaffold. b) SEM images showing the photoresist mold before (i, ii) and after (iii, iv) the reflow process—corresponding to steps 2 and 3 in (a), respectively—in low (i, iii) and high (ii, iv) magnifications. c) SEM images of micropatterned PDMS obtained from photoresist mold before (i, ii) and after (iii, iv) reflow process in low (i, iii) and high magnifications (ii, iv). The inset in (i) shows a flat and a micropatterned substrate with clear and opaque colors on top and bottom, respectively. (Scale bars: 20 μm in (b), (c) i, iii and 5 μm in (b), (c) ii, iv.) d) SEM images of dried mature primary CMs on glass at low (i) and high (ii) magnifications. Bright-field image (iii) and the corresponding fluorescent microscopy image of mature primary CMs on micropatterned PDMS—stage 7 in (a). e) SEM images of (i) the surface of a cell-imprinted substrate and an optical photo in inset showing an indentation with rough bottom surface as the result of cell imprinting, (ii) a dried cell in a micropattern, (iii, iv) cell imprints from cells in micropatterns. Scale bars: 50 μm in (d) i and (e) i, 5 μm in (d) ii, (e) ii–iv, and 100 μm in (d) iii, iv.

plates (Figure 1di,ii) were fixed and used as a mold for creating imprints (Figure 1e). Finally, we combined photolithography and cell imprinting to produce surfaces with imprints of aligned mature CMs. Mature primary human CMs were seeded and aligned on the micropatterned PDMS substrates

(Figure 1diii,iv), fixed, and then used as molds for producing microgrooves with cell topography at the sub-micrometer level (Figure 1e). Hereafter, we use the terms *micropatterned*, *cell-imprinted*, and *multiscale imprinted* substrates for those made, respectively, using photolithography, imprinting of

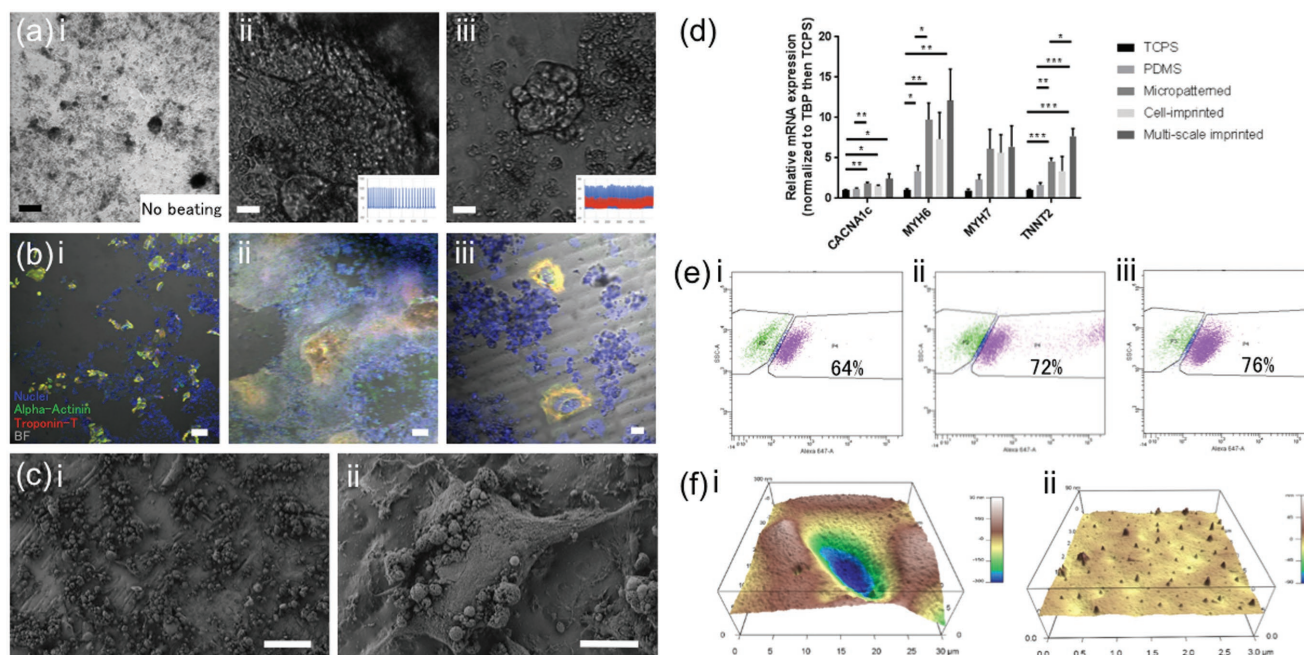


Figure 2. IPSC differentiation on PDMS substrates. a) Still images of Videos S1–S3 (Supporting Information) of beating (or lack of beating) of iPSCs at day 16 of differentiation on unpatterned (i: 4 \times), cell-imprinted (ii: 40 \times), and multiscale imprinted (iii: 40 \times) PDMS substrates. The insets in (ii) and (iii) show the beating signals. Scale bars: 200 μm in (i) and 20 μm in (ii, iii). b) Confocal fluorescent microscopy images of iPSCs at day 13 on unpatterned (i: 10 \times), cell-imprinted (ii: 10 \times), and multiscale imprinted (iii: 40 \times) substrates—merged nuclei (blue), cardiac Troponin T (red), sarcomeric alpha actinin (green), and bright-field (BF, gray). Scale bars: 100 μm in (i), (ii) and 20 μm in (iii). c) SEM images showing iPSCs at day 13 on a multiscale imprinted PDMS substrate at low (i) and high (ii) magnifications. Scale bars: 100 μm in (i) and 20 μm in (ii). d) Expression of genes TNNT2, MYH6, MYH7 (cardiac maturity and contractility), and CACNA1c (Ca^{2+} transport) at day 16 on micropatterned, cell-imprinted, and cell-imprinted PDMS in addition to control groups of TCPS and unpatterned PDMS (mean \pm SEM, normalized to TBP then TCPS, $N = 4/\text{group}$, $*p < 0.05$, $**p < 0.01$, $***p < 0.001$). e) Flow cytometry chart of SSC-A versus Alexa Fluor 647-A for cells from TCPS (i), unpatterned PDMS (ii), and multiscale imprinted PDMS substrate (iii) labeled with Alexa Fluor 647-conjugated mouse monoclonal cardiac Troponin T antibody; the percentages show the ratio of cells that were positive for cardiac Troponin T enclosed in the right boxes; the left boxes show background signal. f) Topography at micro- and sub-microlevel shown by AFM profiles of a cell-imprinted substrate at low (i) and high (ii) magnifications.

randomly oriented primary human cells, and a combination of photolithography and imprinting. We compared the performance of all fabricated scaffolds—micropatterned, imprinted, and multiscale imprinted substrates—in iCM alignment, differentiation, and maturation.

PDMS substrates were explored for use as scaffolds for differentiation of iPSCs. Cells were dissociated from petri dishes and seeded on the three types of substrates; unpatterned PDMS and tissue culture polystyrene (TCPS) served as controls. iPSCs on cell-imprinted and multiscale imprinted substrates were generally the first to begin beating (as early as day 10), indicating differentiation to iCMs. In a typical set, shown in Figure 2a and Videos S1–S3 (Supporting Information) at day 16, iPSCs on unpatterned PDMS do not beat, whereas both cell-imprinted and multiscale imprinted substrates have beating cells on them. Confocal fluorescent images reveal stronger signals associated with cardiac Troponin T and sarcomeric alpha-actinin from the cell-imprinted and multiscale imprinted substrates than from controls (Figure 2b). Scanning electron microscopy (SEM) images of cells on multiscale imprinted substrates show attachment and conformation of cells to the asperities of the surface (Figure 2c). The significant acceleration of the process of development of iPSCs to iCMs using our substrates is quantitatively shown via quantitative polymerase chain reaction (qPCR)

for measurement of expression of genes relevant to cardiac maturity—TNNT2, MYH6, MYH7, and CACNA1c (Figure 2d) and flow cytometry of cells labeled with TNNT2 (Figure 2e). Multiscale imprinted PDMS substrates demonstrated the highest expression of these genes, significantly higher than controls. The percentage of cells labeled with TNNT2 increased from 70% on TCPS to 81 and 84% on unpatterned and cell-imprinted PDMS substrates, respectively. The general positive effect of PDMS on differentiation and maturation of iPSCs is likely due to the low stiffness of the substrate compared to polystyrene. The 3D topography of cell-imprinted PDMS substrates (Figure 2f) is an additional cue that significantly enhances the performance of PDMS substrates.

In the next step, to evaluate the effects of the micropatterned PDMS substrates made by photolithography on alignment and maturation of CMs, we cultured iCMs on them (Figure 3). Beating iCMs were dissociated from polystyrene plates and seeded on sterilized micropatterned PDMS substrates coated with Geltrex. Bright-field and fluorescent photos show a high degree of alignment of iCMs on the patterned substrates as early as day 1 after seeding of cells. Microscopy images taken from the border between the unpatterned and patterned sections of the surface, in particular, clearly show the difference between the orientation and alignment of iCMs on the two sides

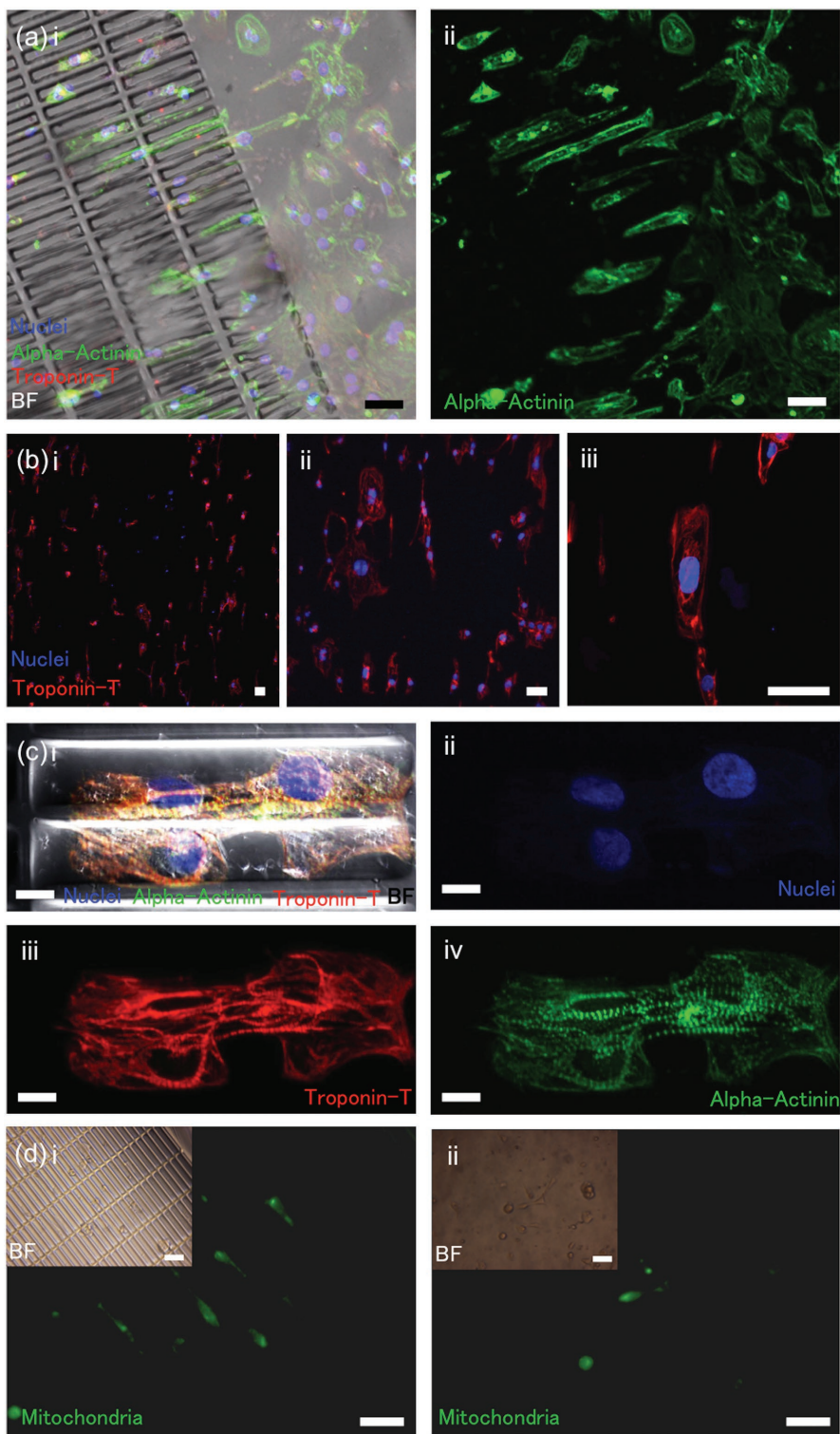


Figure 3. iCMs on micropatterned substrates. a) Confocal images of iCM organization on a PDMS substrate that is half patterned on the left and half unpatterned on the right: (i) merged nuclei (blue), cardiac Troponin T (red), sarcomeric alpha actinin (green), and bright-field (BF, gray), (ii) sarcomeric alpha actinin (green) signal shown only for a clearer illustration of the orientation of cells (Day 7, magnification: 20 \times , scale bars: 50 μm). b) Confocal images of iCM organization on a patterned substrate labeled with cardiac Troponin T (red) and nuclei (blue) at three different magnifications: (i) 10 \times , (ii) 20 \times , and (iii) 60 \times , show the conformation of iCMs to the 3D patterned PDMS (Day 14, scale bars: 50 μm). c) Confocal images of merged with BF (i) and separate nuclei (ii), Troponin T (iii), and sarcomeric alpha actinin (iv) signals from iCMs in two adjacent cell-size patterns (day 14, magnification: 60 \times , scale bars: 10 μm). d) Mitochondria labeled in iCMs on patterned and unpatterned PDMS substrates showing higher magnitude of signal received from those on the patterned substrate and more scarce mitochondria indicated by weaker signal on the unpatterned substrate (day 26, magnification: 10 \times , scale bars: 50 μm).

(Figure 3a and Videos S4 and S5, Supporting Information). Cardiac protein Troponin T—encoded by gene *TNNT2*—plays a critical role in sarcomere assembly and Ca^{2+} activation of cardiac myofilament contraction.^[22] Labeled cardiac Troponin T shows anisotropy in the orientation of the iCMs and their alignment in the direction of patterns. More importantly, they conform to the 3D shape of the microgrooves on the patterned substrates (Figure 3a–c). Maturation of iCMs is evident from the sarcomeric structure, visualized by labeled sarcomeric alpha actinin, which shows myofibril alignment and striated appearance of Z-discs (Figure 3c). Mitochondria are more abundant in the cells on the patterned substrates but more sparse on unpatterned substrates (Figure 3d), demonstrating a higher degree of maturity.^[11b,23]

To further investigate the transition from an unpatterned surface to a fully patterned one, we created wavy features on some substrates that were not as deep as those on the fully patterned substrates (Figure 4a). The wavy features were made by decreasing the distance between the patterns in photoresist; the shorter distance results in partial exposure of the resist between the pattern and does not allow the entire thickness of the photoresist to be removed with developer, hence producing wavy patterns upon reflow. The shorter (1–2 μm) distance produced wavy features, whereas 5–10 μm made fully isolated microstructures. We compared the behavior of cells on the substrates and observed increases in anisotropy in beating (Figure 4b and Videos S6–S8, Supporting Information) and in orientation visualized by cardiac Troponin T (Figure 4c) from the unpatterned to the fully patterned substrate, which has the physiological dimensions of primary mature CMs. Anisotropy is a characteristic feature of CMs in myocardium. Ca^{2+} flow was visualized using a spinning disk microscope, which revealed isotropic flow in the cells on unpatterned surfaces (Figure 4d and Video S9, Supporting Information) and anisotropic flow in the cells on patterned surfaces (Figure 4e,f and Videos S10 and S11, Supporting Information).

To define the mechanisms underlying the superiority of 3D over 2D substrates, we probed variations in cell and nucleus shapes together with their effects on chromatin conformational changes using our recently developed virtual cell model.^[21c] The virtual cell model has the advantage of providing a virtual environment that closely mimics interactions between cell and substrate. During the *in silico* experiments we “turned off” all unwanted chemical interactions and focused on how the geometry of the substrate affects the shaping of the cell. While a smooth substrate led to an isotropic spread of cells (Figure 5a and Video S12, Supporting Information), a patterned substrate elongated the cell significantly (Figure 5b and Video S12, Supporting Information). While a cell on a smooth substrate is free to spread isotropically (see Figure 5c), our results (at all time points of the *in silico* experiments) show that cells spreading on patterned substrates strongly favor the direction of the patterns, hence elongating along the patterns. Figure 5d demonstrates the very small deviation angle in the direction of cell polarization (red strip) from the elongation direction (here designated zero) during the simulation. As a comparison, when cells are allowed to spread on a smooth substrate, the strip grows to covers all angles (gray).

The virtual cell model also paints a picture of how chromatin chain conformation is affected by the substrate during spreading. Chromatin fibers with a looped shape ($N = 10$) were placed inside the nucleus and their contact points with each other and other loops were monitored during spreading. We found that the nucleus shape is affected by the spreading process, confining it to a smaller volume than would be possible in a suspended cell. Additionally, a patterned substrate further confines the nucleus, limiting the chromatin to a smaller volume. As a result, more chromatin fiber segments are in contact with each other in the nucleus when the cell spreads on the patterned substrate (see Figure 5e) as compared to the smooth substrate (see Figure 5f). The graph assigns digits to each of the chromatin filament segments and displays the number of times segments on different chromatin loops “touch” each other.

3. Discussion

Culturing cells on patterned surfaces has long been known to affect cell morphology and behavior.^[24] Even surfaces generally considered smooth (such as glass) have surface heterogeneities that influence the morphology of spreading cells.^[15b,25] The creation of larger, “cell-scale” patterns allows for the preferential alignment of cells (in some cases independent of certain measurements of macroscopic surface energy changes) due to their confinement in the patterns.^[26] Therefore, the changes in cell shape that are governed by such surface heterogeneities serve as epigenetic cues to control cellular behavior such as gene signaling and cell migration.^[27] This has been confirmed not only by the use of patterns but also surface roughness in general, which influences cell adhesion and behavior in many different systems.^[28] Such control of cell fate depends on the physical and mechanical cues the cell receives from the microenvironment, which guide embryonic development as well as adult tissue formation and function.^[29] The engineering of surface topography to provide an environment that mimics the cell’s native context has therefore been exploited for medical purposes, including tissue engineering and drug screening, using many cell types.^[30] Because of their similarity to native extracellular matrix, surfaces designed using 3D patterns formed using photolithography are superior to 2D patterns in producing cells with mature morphological features.

Adult cardiac CMs have many mature features absent from iCMs cultured on 2D substrates. iCMs cultured on 2D substrates typically express cytoskeletal proteins and mitochondrial distribution more similar to neonatal than mature CMs.^[31] We showed that a 3D micropatterned substrate produced alignment of CMs and their sarcomeric structures, as well as more-distinguishable mitochondrial distribution, both characteristic of mature CMs. Combined with more-mature calcium-signaling characteristics, this suggests that the internal structure of the cell was influenced by the cylindrical shape typical of mature CMs. CMs reorganize their cytoskeletal network according to physico-mechanical signals from the microenvironment. The cylindrical shape of the CM, dictated here by the 3D patterns, influences sarcomeric structure and consequently, contractility. Furthermore, the 3D cell shape alters the shape of the nucleus

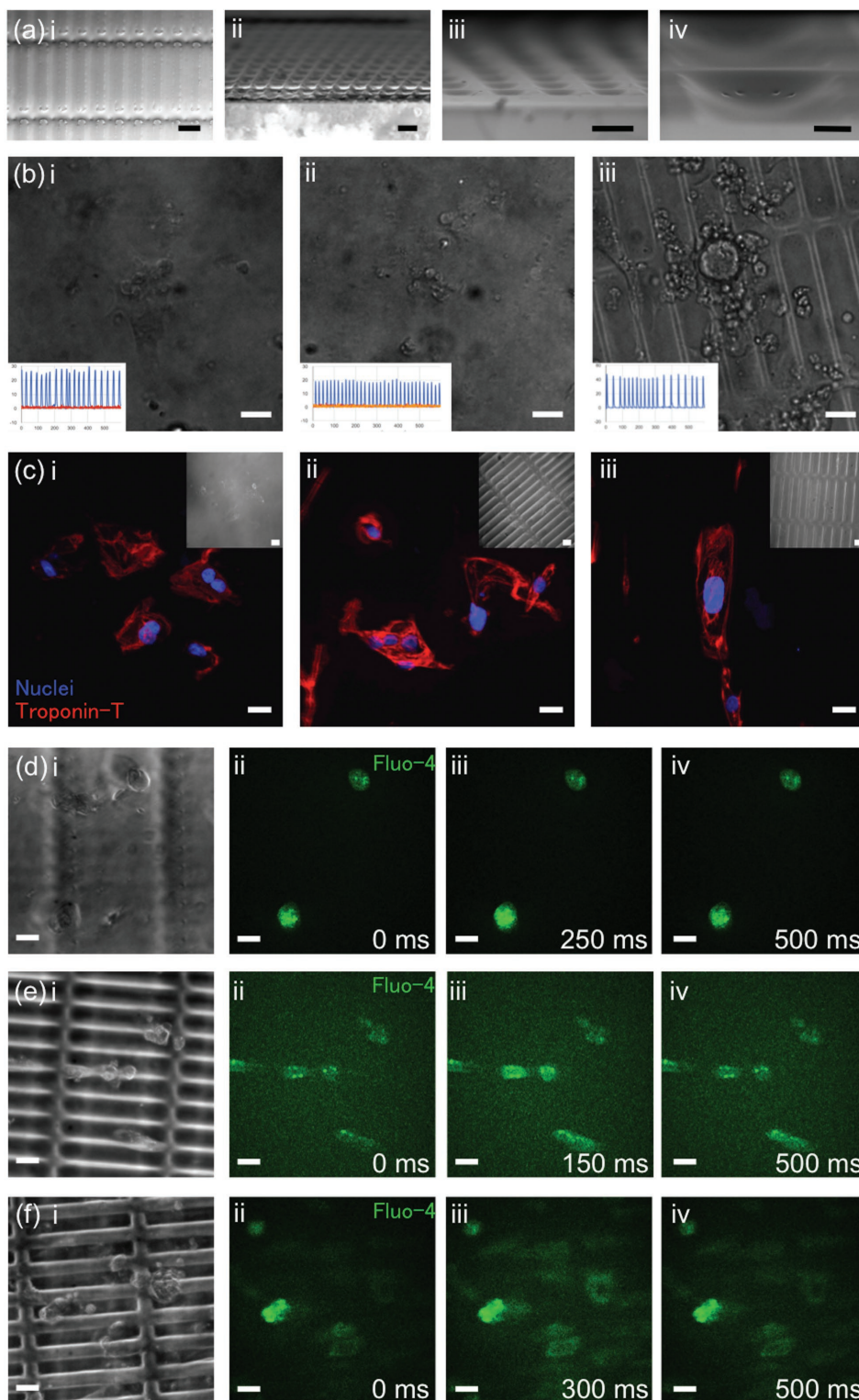


Figure 4. Gradual change of topography from unpatterned to micropatterned and its effect on the behavior of iCMs. a) SEM images of wavy (i, ii) and fully micropatterned (iii, iv) PDMS substrates. Scale bars: 20 μm in (i)–(iii) and 5 μm in (iv). b) Still images of Videos S6–S8 (Supporting Information) of beating of iCMs at day 26 on unpatterned (i), wavy (1 μm) (ii), and fully micropatterned (10 μm) (iii) PDMS substrates. The insets show the beating signals. Magnification: 40 \times . Scale bars: 20 μm . c) Confocal fluorescent microscopy images of iCMs at day 14 on unpatterned (i), wavy (2 μm) (ii), and fully micropatterned (iii) PDMS substrates—merged nuclei (blue) and cardiac Troponin T (red). Bright-field images are shown in insets. Magnification: 60 \times . Scale bars: 20 μm . Ca^{2+} flow traced by Fluo-4 dye on d) wavy (1 μm), e) fully patterned (5 μm), and f) fully patterned (10 μm) PDMS substrates: (i) shows bright-field image and (ii)–(iv) show snapshots of Videos S9–S11 (Supporting Information) at various times. Magnification: 40 \times . Scale bars: 20 μm .

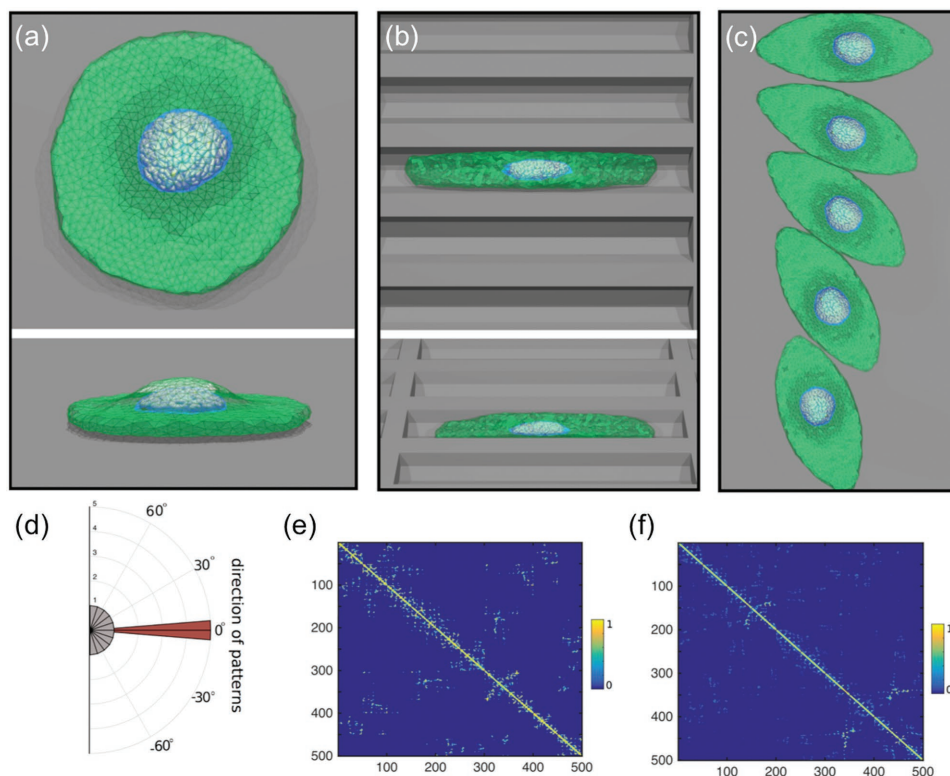


Figure 5. Virtual cell predicts cardiomyocyte behavior on substrates. a) Top and side view of virtual cell spread on a smooth surface. During the early stages of the spreading process the cell has a symmetrical form. b) Here, we have the same cell as in (a), spread on a patterned substrate. c) A cell that (after attachment to a smooth substrate) has polarized in a random direction. The direction of the polarization will change with angular noise over time. d) The deviation of the angle of polarization vector of the cell from the direction of the patterned substrate after cell attachment. e) The number fraction of contacts between different chromatin fiber segments measured after the cell has spread on a patterned surface. The color yellow (blue) indicates that two segments, associated by the coordinates on the graph, were (were not) in contact with each other throughout the simulation. f) The same contact matrix as in (e), for the cell that has spread on a smooth substrate.

via the linker of nucleoskeleton and cytoskeleton (LINC) complex—proteins connecting nuclear lamina to cytoskeleton—thus regulating chromatin conformation and gene expression.^[32] To further confirm these results, we utilized a virtual cell model designed to manipulate the iCMs' mechanical properties. We focused on the mechanical interactions between the iCMs and the substrate and showed that the patterned substrate guides the cells to spread and elongate along the pattern. Also, mathematical analysis allowed us to monitor the conformation of the chromatin fibers in the nucleus and showed that their contact points are more stable when the cell is on a patterned substrate.

We further combined 3D topographical features with cell imprinting to further enrich surface detail, giving iCM a more-mature morphology, and thus greater physiological functionality. In this case, the cytoskeletal network is reorganized upon sensing physico-mechanical signals from the environment at the sub-micrometer level, which promotes differentiation and maturation. These effects could be traced down to the level of gene expression, as revealed by qPCR and fluorescent staining experiments showing the enhanced maturity of iCMs cultured on cell-imprinted substrates. From a macroscale standpoint, we showed that the addition of specific 3D topographical features improved the physiological morphology of CMs similar to what previous studies have shown with other cell types.^[33]

We hypothesized that the imprinted substrate would provide an “adhesive map” to guide the iPSCs membrane toward native CM features ranging from gene expression to gross morphology, producing iCMs more similar to natural CMs. Our results confirmed this hypothesis (Figures 2–5). Therefore, cell imprinting technology can be used to enhance the maturity of iCMs when combined with 3D geometrical topographical features, possibly leading to more effective treatments in the field of cardiac regeneration.

4. Conclusion

We fabricated PDMS substrates with cell-scale micropatterns, cell-imprinted topography, and a combination of both. The multiscale imprinted substrates were the most effective in accelerating the process of differentiation of iPSCs and producing mature CMs. We also showed that cell-scale micropatterns made using photolithography are highly effective in eliciting maturation of iCMs and developing cells with the geometry and functionality of adult mature CMs. We relate the effect of topography on the differentiation and maturation of iCMs to reorganization of cytoskeleton and regulation of chromatin conformation and gene expression via the LINC complex. All these changes spring from biomechanical and biophysical cues

communicated to the cells through interactions with the topographical features of the microenvironment.

5. Experimental Section

Fabrication of Multiscale-Patterned Substrates: CM scaffolds with 3D imprints of aligned mature CMs were fabricated using a four-step process:

1. *Hard Micropatterned Master Mold:* Hard master molds mimicking the shape and alignment of mature cardiomyocytes in adult human myocardium were fabricated via UV photolithography. 4 in. silicon wafers (University Wafers, Boston, MA) were washed with acetone and isopropanol prior to spin-casting AZ P4620 (AZ Electronic Materials, Branchburg, NJ) at 3500 rpm for 40 s to achieve 7–8 μm thickness. The coated wafers were subsequently soft baked at 115 $^{\circ}\text{C}$ for 2 min. Patterns of aligned rectangles with a dimension of 16 μm \times 100 μm —the average size of a mature human CM—and a pitch of 17–26 μm to create gap distances ranging 1–10 μm were made on a chrome-coated glass photomask using an MW1 Heidelberg photomask writer (Heidelberg Instruments, Germany). The pattern was transferred to the photoresist using the MJB-4 contact aligner (SUSS Microtec AG, Germany) with 400–600 mJ cm^{-2} exposure energy, followed by developing with AZ 300 MIF for 3 min, then rinsing with water. To eliminate the sharp edges of the micromolds and create semicircular cross-sectional areas similar to the 3D cylindrical shape of native CMs, photoresist reflow was induced through heat treatment at 150 $^{\circ}\text{C}$ for 30 min. The reflow capability was the reason for choosing a positive photoresist instead of the more commonly used SU-8, which is a negative photoresist. In the latter, the pattern remaining after developing is made of cross-linked photoresist, which because of its high glass transition temperature (T_g) is not an appropriate candidate for the reflow process. However, a positive photoresist is reflowable, as the cross-linked polymer is removed in the developing process and the remaining pattern has a significantly lower T_g .

2. *Soft Micropatterned PDMS Mold:* The hard master molds made in step 1 were used to fabricate soft PDMS molds with aligned hollow CM-shaped patterns. PDMS prepolymer and curing agent were mixed in a 10:1 ratio, stirred, and degassed for 30 s each in a THINKY mixer AR-100 (THINKY USA, Inc., Laguna Hills, CA). The degassed mixture was poured onto the master molds made in step 1 and placed in an oven at 65 $^{\circ}\text{C}$ for 2 h. PDMS was then detached from the master mold and cut into pieces for cell culture in step 3.

3. *Multiscale-Patterned Primary Cell Mold:* To construct the sub-micrometer structure of myofibrils in CMs, primary human mature CMs aligned on the micropatterned molds made in step 2 were used. Primary human cardiomyocytes (PromoCell GmbH, Heidelberg, Germany) were thawed and seeded on the PDMS molds fabricated in step 2 with a cell density of 20k cm^{-2} . For preparation of substrates for seeding, the substrates were washed in 70% ethanol and then exposed to UV overnight. The medium suggested by the supplier, which contains 5% v/v FCS and 5 $\mu\text{g mL}^{-1}$ insulin, was changed every 3 d. After 14 d of culture, when the majority of cells exhibited mature cardiomyocyte markers, cells were fixed in 4% paraformaldehyde and immediately used as molds in step 4.

4. *Multiscale-Patterned and Cell-Imprinted PDMS Mold:* PDMS—prepared according to the method described in step 2—was poured onto the fixed primary cells. The PDMS and cells were placed in a 37 $^{\circ}\text{C}$ incubator overnight. The resulting PDMS after detachment showed an overall configuration of aligned CMs directed by the mold fabricated in steps 1 and 2 as well as sub-micrometer-level asperities of CMs produced by the mature cell imprinting in steps 3 and 4. Before seeding of cells, the substrates were washed in 1% NaOH in a shaker and then sterilized under UV.

Atomic Force Microscopy (AFM): Topographic images were taken using an Asylum Cypher AFM in noncontact (AC) mode. A tapered rectangular silicon probe with an apex tip—AC240BSA-R3 (Oxford Instruments, CA), $f = 75 \text{ Hz}$, $k = 2 \text{ N m}^{-1}$ —was used. Images of 30 μm \times 30 μm or 3 μm \times 3 μm

areas were obtained by scanning 256 lines at the resolution of 256 points with a scan rate of 1.24 Hz.

iPSC Culture and Differentiation to CM: BJRiPS (Harvard Stem Cell Institute, Cambridge, MA) were cultured in 10 cm cell-culture-treated petri dishes after incubation at 37 $^{\circ}\text{C}$ with 8 mL of Geltrex (Thermo Fisher, NY, USA, 100 \times diluted in DMEM) for half an hour, removing the excess solution, and adding 10 mL of complete mTeSR1 (STEMCELL Technologies Inc., Cambridge, MA) with 1% pen/strep (Thermo Fisher). mTeSR1 containing 5 $\times 10^{-6}$ M ROCK inhibitor (Selleck Chemicals, TX, USA, Y27632) was used after thawing the cells and removed the next day, whereupon fresh mTeSR1 with no inhibitor was added. iPSCs were maintained at 37 $^{\circ}\text{C}$ with 5% CO_2 , and medium was changed daily until cells reached $\approx 80\%$ confluence. Cells were passaged by adding 5 mL of Gentle Cell Dissociation Reagent (STEMCELL Technologies Inc., Cambridge, MA) and incubating for 6 min at 37 $^{\circ}\text{C}$. The reagent was then removed and replaced with mTeSR1 containing ROCK inhibitor, and a cell scraper was used to detach the cells and split them at an approximate ratio of 1 to 3.

For differentiation of iPSCs into CM, 500 μL of Geltrex (100 \times diluted) was added to each well of a 12-well tissue culture polystyrene plate and allowed to gel, as described previously. iPSCs were then added at a concentration of 500k cells per well with 2 mL of mTeSR1 containing ROCK inhibitor. When iPSCs were confluent, cell-culture medium was removed and RPMI/B27 (Thermo Fisher, NY, USA, containing glucose, no insulin, 1% pen/strep) with 12 $\times 10^{-6}$ M CHIR99021 (Selleck Chemicals, TX, USA) was added to each well (day 0). On day 1 the medium was changed to RPMI/B27. On day 3 half of the cell medium was removed and mixed 1:1 with fresh medium before adding 5 $\times 10^{-6}$ M IWP4 (Stemgent Inc., MA, USA). After 2 d, the medium was changed to fresh RPMI/B27, and after an additional 2 d (day 7), RPMI/B27 with 10 $\mu\text{g mL}^{-1}$ of insulin (Sigma Aldrich, MA, USA) was added. Medium was then changed every 3 d with RPMI/B27 containing insulin. For differentiation experiments, iPSCs were plated onto substrates prior to chemical differentiation per the above protocol. For maturation experiments, iPSCs were first differentiated on TCPS then dissociated with TrypLE and replated onto the substrates once beating commenced after at least 14 d of differentiation.

Cell Characterization: Fluorescence Microscopy of CMs: Cells were first washed with phosphate-buffered saline (PBS, Sigma Aldrich, MO, USA) and fixed with a 4% paraformaldehyde (PFA) solution (Sigma Aldrich, MO, USA) for 30 min at room temperature followed by three 5 min washes with PBS. Cells were then permeabilized with 0.1% triton X-100 for 30 min at room temperature. After washing with PBS (again, three times for 5 min each) cells were incubated with 10% goat serum-blocking solution. After overnight incubation at 4 $^{\circ}\text{C}$ with primary antibodies— α -actinin mouse (Sigma Aldrich, MO, USA) and C Troponin-T rabbit (Abcam, MA, USA)—at a concentration of 1:400 in 2% goat serum, cells were washed with PBS (three times, 10 min each). Secondary antibodies—Alexa Fluor 488 Goat Anti-Mouse IgG (H+L) and Alexa Fluor 594 Goat Anti-Rabbit IgG (H+L) (Life Technologies, MA, USA)—were then added for 1 h at room temperature prior to washing with PBS (three times, 10 min each). Before imaging, the cells were incubated for 30 min at room temperature with Dapi (Life Technologies, MA, USA) at a concentration of 2 drops mL^{-1} . Samples were then visualized using a FV1000 confocal fluorescent microscope.

Live Imaging of Ca^{2+} Flow, Beating Behavior, and Mitochondria: Ca^{2+} signaling and beating behavior were captured using an Andor Revolution Spinning Disk Microscope. For imaging of Ca^{2+} signaling, a Fluo-4 NW Calcium Assay Kit (Thermo Fisher Scientific, MA, USA) was used according to manufacturer's protocol. Cells were incubated with Fluo-4, a green-fluorescent calcium-indicator dye, for 30 min at 37 $^{\circ}\text{C}$. The dye solution was subsequently replaced with fresh medium before imaging. Cells were then held at physiological conditions during imaging and video recording. A 488 nm laser line and bright-field mode were used for capturing Ca^{2+} flow and beating, respectively. The beating profiles were extracted from videos using the commercial software Cellogy (Cellogy Inc., CA, USA). CellLight Mitochondria-GFP, BacMam 2.0 (Thermo Fisher Scientific, MA, USA) was utilized for labeling of mitochondria with

green fluorescent protein (GFP) in live cells. Cells were incubated with the dye solution overnight and then imaged using an EVOS fluorescence microscope.

Quantitative Polymerase Chain Reaction: For qPCR, a Cells-to-CT 1-step TaqMan kit (Thermo Fisher Scientific, MA, USA) was used according to the manufacturer's instructions. Briefly, cells were first washed with PBS, and lysis buffer was introduced, followed by pipetting five times; then they were allowed to incubate for 5 min at room temperature. The stop solution was then mixed into the lysate and allowed to incubate for 2 min before being placed on ice or stored at -20°C . The lysates, master mix, and Taqman probes were mixed into a 384-well plate, followed by vortexing for 10 s and centrifuging. Manufacturer recommendations were then followed for thermal cycling. Taqman probes, TBP (housekeeping), TNNT2, MYH6, MYH7 (cardiac maturity and contractility), and CACNA1c (Ca^{2+} transport) were examined. Expression of each transcript was normalized with respect to the housekeeping gene. Mean cycle threshold (C_t) was calculated, and ΔC_t was calculated as each gene's mean C_t value minus the mean C_t value of the control. Fold of expression was calculated according to the formula: $2^{(-\Delta C_t)}$.

Flow Cytometry: iCMs were dissociated and fixed with 1% PFA for 20 min, then permeabilized with cold 90% methanol for 15 min. Cells (1×10^6 in 1 mL) were then rinsed and incubated with Alexa Fluor 647-conjugated mouse monoclonal TNNT2 antibody (Thermo Fisher Scientific, MA, USA) for 1 h. Cells were filtered through a 100 μm cell strainer, then analyzed via a BD FACSAria III flow cytometer.

Scanning Electron Microscopy: SEM images were taken using a Zeiss SEM. For cell imaging, cells were washed and fixed with 2% glutaraldehyde solution (Sigma Aldrich, MO, USA) in 50×10^{-3} M Na-cacodylate buffer (Sigma Aldrich, MO, USA). Cells were allowed to fix for 1 h at room temperature, then dehydrated in a graded ethanol dehydration process: 50, 70, 80% for 10 min each; 95% (two times, 5 min each); and 100% (three times, 5 min each). Samples were coated with 5 nm of Pt/Pd using a sputter coater prior to imaging. Photoresist molds and PDMS substrates were also coated with 5 nm of Pt/Pd prior to imaging.

Image Processing: The brightness and contrast in the microscopy images obtained using fluorescence microscopes and SEMs were adjusted off-line in Microsoft PowerPoint whenever needed to improve clarity. The adjustments were made equally across the entire image and equally in the controls.

The Virtual Cell Model: The virtual cell model comprises four main parts: the membrane, the cytoskeleton, the chromatin fibers, and the substrate. Each part acts as an independent variable that is fine-tuned to behave like the iCMs used in *in vivo* experiments (50). There are many ways in which the iCM may interact with the substrate, and we have the advantage of removing any unwanted influence (such as chemical reactions) to isolate the effects that are the focus of the study.

Measuring the Anisotropy of the In Silico Experiments: The virtual cell model was programmed to break symmetry (if required) upon attachment to substrate. If the cell senses no barriers that are energy costly, it will acquire a random direction and break symmetry (elongate) along that direction. However, the cell will not settle on a specific direction and will change its polarization with an angular noise during the simulation. Given enough time, the cell will spread in all directions on a smooth, open substrate (see Figure 5c). The cell polarization vector was monitored and the angle it makes with the patterns on the substrate (based on the orientation of the patterns) was measured after the cell is successfully attached to the substrate and the spreading process begins.

Chromatin Contact Matrix: Each chromatin chain confined in the nucleus was divided into 50 segments, and each assigned a digit. During any chosen stage of the simulation, the number of times each segment contacts another and whether they belong to the same chromatin fiber or otherwise, was counted over a specific time period. This procedure was carried out during three stages of the simulation: while the cell was suspended above the substrate, while the cell was attached to the smooth substrate, and while the cell was attached to the patterned substrate. The color of each point on the graph in Figure 5e,f represents the contact number fraction during each stage as specified by the graph

title. The coordinates of each point reflect the segment number labels that were in contact at that specified time.

Supporting Information

Supporting Information is available from the Wiley Online Library or from the author.

Acknowledgements

The authors gratefully acknowledge funding from the U.S. National Institutes of Health (NIH) Grant Nos. HL127464-01A1 (O.C.F.), EB015419 (O.C.F.), and Department of Defense Grant No. PC140318 (O.C.F.). P.P.S.S.A. was supported by NIH Grant No. 5T32EB016652-02 and American Heart Association Grant No. 17SDG33660925. J.C.G. was supported by the John S. LaDue Memorial Fellowship in Cardiology from Harvard Medical School. This work was performed in part at the Center for Nanoscale Systems (CNS), a member of the National Nanotechnology Coordinated Infrastructure Network (NNCI), which was supported by the National Science Foundation under NSF Award No. 1541959. CNS is part of Harvard University. The authors thank the Neurobiology Department and the Neurobiology Imaging Facility for consultation and instrument availability that supported this work. That facility was supported in part by the Neural Imaging Center as part of an NINDS P30 Core Center Grant No. NS072030.

Conflict of Interest

O.C.F. declare financial interests in Selecta Biosciences, Tarveda Therapeutics and Placon Therapeutics.

Keywords

cell imprinting, induced pluripotent stem cells, mature cardiomyocytes, polydimethylsiloxane, surface topography

Received: December 19, 2017

Revised: February 1, 2018

Published online: March 13, 2018

- [1] A. L. Bui, T. B. Horwich, G. C. Fonarow, *Nat. Rev. Cardiol.* **2011**, *8*, 30.
- [2] a) M. Mahmoudi, M. Yu, V. Serpooshan, J. C. Wu, R. Langer, R. T. Lee, J. M. Karp, O. C. Farokhzad, *Nat. Nanotechnol.* **2017**, *12*, 845; b) A. Tachibana, M. R. Santoso, M. Mahmoudi, P. Shukla, L. Wang, M. Bennett, A. B. Goldstone, M. Wang, M. Fukushi, A. Ebert, *Circ. Res.* **2017**, *121*, 22.
- [3] K. Kikuchi, K. D. Poss, *Annu. Rev. Cell Dev. Biol.* **2012**, *28*, 719.
- [4] M. N. Hirt, A. Hansen, T. Eschenhagen, *Circ. Res.* **2014**, *114*, 354.
- [5] a) J. Taupitz, *Eur. Rev.* **2017**, *25*, 121; b) S. Yamanaka, *Cell Stem Cell* **2012**, *10*, 678.
- [6] a) P. S. Knoepfler, *Stem Cells* **2009**, *27*, 1050; b) Z. Liu, Y. Tang, S. Lü, J. Zhou, Z. Du, C. Duan, Z. Li, C. Wang, *J. Cell. Mol. Med.* **2013**, *17*, 782; c) P. J. Kim, M. Mahmoudi, X. Ge, Y. Matsuura, I. Toma, S. Metzler, N. G. Kooreman, J. Ramunas, C. Holbrook, M. V. McConnell, *Circ. Res.* **2015**, *116*, e40.
- [7] a) A. A. Youssef, E. G. Ross, R. Bolli, C. J. Pepine, N. J. Leeper, P. C. Yang, *JACC* **2016**, *1*, 510; b) P. W. Burridge, Y. F. Li, E. Matsa, H. Wu, S.-G. Ong, A. Sharma, A. Holmström, A. C. Chang,

- M. J. Coronado, A. D. Ebert, *Nat. Med.* **2016**, *22*, 547; c) A. Sharma, P. W. Burrige, W. L. McKeithan, R. Serrano, P. Shukla, N. Sayed, J. M. Churko, T. Kitani, H. Wu, A. Holmström, *Sci. Transl. Med.* **2017**, *9*, eaaf2584.
- [8] a) Y. Tanaka, K. Morishima, T. Shimizu, A. Kikuchi, M. Yamato, T. Okano, T. Kitamori, *Lab Chip* **2006**, *6*, 362; b) V. A. Webster, E. L. Hawley, O. Akkus, H. J. Chiel, R. D. Quinn, *Biomimetic and Biohybrid Systems, Living Machines 2015*, Vol 9222 (Eds: S. Wilson, P. Verschure, A. Mura, T. Prescott), Lecture Notes in Computer Science, Springer, Cham.
- [9] a) J. Dow, B. Z. Simkhovich, L. Kedes, R. A. Kloner, *Cardiovasc. Res.* **2005**, *67*, 301; b) K. Cheng, D. Shen, M. T. Hensley, R. Middleton, B. Sun, W. Liu, G. De Couto, E. Marbán, *Nat. Commun.* **2014**, *5*, 4880.
- [10] a) M. A. Bray, S. P. Sheehy, K. K. Parker, *Cytoskeleton* **2008**, *65*, 641; b) S. D. Lundy, W.-Z. Zhu, M. Regnier, M. A. Laflamme, *Stem Cells Dev.* **2013**, *22*, 1991; c) F. S. Korte, T. J. Herron, M. J. Rovetto, K. S. McDonald, *Am. J. Physiol.* **2005**, *289*, H801; d) J. Schaper, E. Meiser, G. Stämmeler, *Circ. Res.* **1985**, *56*, 377.
- [11] a) M. Gherghiceanu, L. Barad, A. Novak, I. Reiter, J. Itskovitz-Eldor, O. Binah, L. Popescu, *J. Cell. Mol. Med.* **2011**, *15*, 2539; b) X. Yang, L. Pabon, C. E. Murry, *Circ. Res.* **2014**, *114*, 511; c) D. J. Lundy, D. S. Lee, P. C. Hsieh, *Ann. Transl. Med.* **2017**, *5*.
- [12] A. Sepac, K. Si-Tayeb, F. Sedlic, S. Barrett, S. Canfield, S. A. Duncan, Z. J. Bosnjak, J. W. Lough, *Cell Transplant.* **2012**, *21*, 2523.
- [13] a) D. Sirabella, E. Cimetta, G. Vunjak-Novakovic, *Exp. Biol. Med.* **2015**, *240*, 1008; b) I. Y. Chen, E. Matsa, J. C. Wu, *Nat. Rev. Cardiol.* **2016**, *13*, 333.
- [14] a) R. G. Harrison, *Science* **1911**, *34*, 279; b) M. J. Dalby, N. Gadegaard, R. Tare, A. Andar, M. O. Riehle, P. Herzyk, C. D. Wilkinson, R. O. Oreffo, *Nat. Mater.* **2007**, *6*, 997; c) O. Mashinchian, L.-A. Turner, M. J. Dalby, S. Laurent, M. A. Shokrgozar, S. Bonakdar, M. Imani, M. Mahmoudi, *Nanomedicine* **2015**, *10*, 829.
- [15] a) S. B. Carter, *Nature* **1967**, *213*, 256; b) P. Weiss, *Int. Rev. Cytol.* **1958**, *7*, 391; c) G. Dunn, J. Heath, *Exp. Cell Res.* **1976**, *101*, 1.
- [16] H. T. H. Au, B. Cui, Z. E. Chu, T. Veres, M. Radisic, *Lab Chip* **2009**, *9*, 564.
- [17] a) E. Cukierman, R. Pankov, D. R. Stevens, K. M. Yamada, *Science* **2001**, *294*, 1708; b) B. M. Baker, C. S. Chen, *J. Cell Sci.* **2012**, *125*, 3015.
- [18] a) F. H. Dickey, *Proc. Natl. Acad. Sci. USA* **1949**, *35*, 227; b) K. Ren, R. N. Zare, *ACS Nano* **2012**, *6*, 4314.
- [19] a) R. Schirhagl, E. W. Hall, I. Fuereder, R. N. Zare, *Analyst* **2012**, *137*, 1495; b) J. Medlock, A. A. Das, L. A. Madden, D. J. Allsup, V. N. Paunov, *Chem. Soc. Rev.* **2017**, *46*, 5110.
- [20] a) M. Mahmoudi, S. Bonakdar, M. A. Shokrgozar, H. Aghaverdi, R. Hartmann, A. Pick, G. Witte, W. J. Parak, *ACS Nano* **2013**, *7*, 8379; b) O. Mashinchian, S. Bonakdar, H. Taghinejad, V. Satarifard, M. Heidari, M. Majidi, S. Sharifi, A. Peirovi, S. Saffar, M. Taghinejad, *ACS Appl. Mater. Interfaces* **2014**, *6*, 13280; c) S. Bonakdar, M. Mahmoudi, L. Montazeri, M. Taghipoor, A. Bertsch, M. A. Shokrgozar, S. Sharifi, M. Majidi, O. Mashinchian, M. H. Sekachaei, *ACS Appl. Mater. Interfaces* **2016**, *8*, 13777.
- [21] a) A. Pierres, A.-M. Benoliel, P. Bongrand, *Eur. Cells Mater.* **2002**, *3*, 31; b) A. Pierres, A.-M. Benoliel, D. Touchard, P. Bongrand, *Biophys. J.* **2008**, *94*, 4114; c) T. Heydari, M. Heidari, O. Mashinchian, M. Wojcik, K. Xu, M. J. Dalby, M. Mahmoudi, M. R. Ejtehadi, *ACS Nano* **2017**, *11*, 9084.
- [22] a) A. J. Sehnert, A. Huq, B. M. Weinstein, C. Walker, M. Fishman, D. Y. R. Stainier, *Nat. Genet.* **2002**, *31*, 106; b) L. S. Tobacman, *Annu. Rev. Physiol.* **1996**, *58*, 447; c) T. Kobayashi, R. J. Solaro, *Annu. Rev. Physiol.* **2005**, *67*, 39.
- [23] J. Piquereau, F. Caffin, M. Novotova, C. Lemaire, V. Veksler, A. Garnier, R. Ventura-Clapier, F. Joubert, *Front. Physiol.* **2013**, *4*, 102.
- [24] P. K. Kreeger, L. E. Strong, K. S. Masters, *Annu. Rev. Biomed. Eng.* **2018**, *20*, 49.
- [25] A. Curtis, C. Wilkinson, *Biomaterials* **1997**, *18*, 1573.
- [26] a) E. Den Braber, J. De Ruijter, H. Smits, L. Ginsel, A. Von Recum, J. Jansen, *J. Biomed. Mater. Res., Part A* **1995**, *29*, 511; b) J. A. Schmidt, A. F. von Recum, *Biomaterials* **1992**, *13*, 675.
- [27] a) J. Dow, P. Clark, P. Connolly, A. Curtis, C. Wilkinson, *J. Cell Sci.* **1987**, *1987*, 55; b) M. J. Dalby, M. O. Riehle, S. J. Yarwood, C. D. Wilkinson, A. S. Curtis, *Exp. Cell Res.* **2003**, *284*, 272; c) L. Chou, J. D. Firth, V.-J. Uitto, D. M. Brunette, *J. Cell Sci.* **1995**, *108*, 1563.
- [28] a) D. D. Deligianni, N. D. Katsala, P. G. Koutsoukos, Y. F. Missirlis, *Biomaterials* **2000**, *22*, 87; b) J. Martin, J. Schwartz, T. Hummert, D. Schraub, J. Simpson, J. Lankford, D. Dean, D. Cochran, B. Boyan, *J. Biomed. Mater. Res., Part A* **1995**, *29*, 389; c) Z. Schwartz, J. Martin, D. Dean, J. Simpson, D. Cochran, B. Boyan, *J. Biomed. Mater. Res., Part A* **1996**, *30*, 145; d) C. Xu, F. Yang, S. Wang, S. Ramakrishna, *J. Biomed. Mater. Res., Part A* **2004**, *71*, 154.
- [29] K. H. Vining, D. J. Mooney, *Nat. Rev. Mol. Cell Biol.* **2017**, *18*, 728.
- [30] a) K. Saha, Y. Mei, C. M. Reisterer, N. K. Pyzocha, J. Yang, J. Muffat, M. C. Davies, M. R. Alexander, R. Langer, D. G. Anderson, *Proc. Natl. Acad. Sci. USA* **2011**, *108*, 18714; b) Y. Ito, *Biomaterials* **1999**, *20*, 2333; c) Y. Lu, A. A. Aimetti, R. Langer, Z. Gu, *Nat. Rev. Mater.* **2016**, *2*, 16075.
- [31] T. Yu, S. Miyagawa, K. Miki, A. Saito, S. Fukushima, T. Higuchi, M. Kawamura, T. Kawamura, E. Ito, N. Kawaguchi, *Circ. J.* **2013**, *77*, 1297.
- [32] S. G. Alam, Q. Zhang, N. Prasad, Y. Li, S. Chamala, R. Kuchibhotla, B. Kc, V. Aggarwal, S. Shrestha, A. L. Jones, S. E. Levy, K. J. Roux, J. A. Nickerson, T. P. Lele, *Scientific Reports* **2016**, *6*, 38063.
- [33] A. M. Greiner, B. Richter, M. Bastmeyer, *Macromol. Biosci.* **2012**, *12*, 1301.